Neural Fields: Localised States with Piece-Wise Constant Interactions

Aytül Gökçe, Stephen Coombes, and Daniele Avitabile

Abstract Neural field models are typically cast as continuum integro-differential equations for describing the idealised coarse-grained activity of populations of interacting neurons. For smooth Mexican hat kernels, with short-range excitation and long-range inhibition, these non-local models can support various localised states in the form of spots in two-dimensional media. In recent years, there has been a growing interest in the mathematical neuroscience community in studying such models with a Heaviside firing rate non-linearity, as this often allows substantial insight into the stability of stationary solutions in terms of integrals over the kernels. Here we consider the use of piece-wise constant kernels that allow the explicit evaluation of such integrals. We use this to show that azimuthal instabilities are not possible for simple piece-wise constant Top Hat interactions, whilst they are easily realised for piece-wise constant Mexican hat interactions.

1 Introduction

Since the 1970s, there has been much progress in developing analytical and numerical techniques to understand brain function and the nervous system. The cortex, being the most complex part of this system, is interconnected by numerous cortico-cortical fibers ($\sim 10^{10}$), whose axon length ranges from 0.5 to 3 mm [17]. Due to its large surface area ($\sim$ 1600–4000 cm^2 in total) with a small thickness ($\sim$ 3 mm), the cortex is often regarded as a two-dimensional laminar structure [12, 17]. Neural field modelling, in both one and two dimensions, is a very well-known framework for approximating the coarse-grained dynamics of a real cortex [8]. It assumes that various classes of neuron types in different cortical layers and areas can be divided into two main sub-populations of neurons (excitatory

A. Gökçe (✉) · S. Coombes · D. Avitabile
School of Mathematical Sciences, The University of Nottingham, University Park, NG7 2RD Nottingham, UK
e-mail: Aytul.Gokce@nottingham.ac.uk; Stephen.Coombes@nottingham.ac.uk; Daniele.Avitabile@nottingham.ac.uk

G. Naldi, T. Nieus (eds.), *Mathematical and Theoretical Neuroscience*,
Springer INdAM Series 24, https://doi.org/10.1007/978-3-319-68297-6_7

and inhibitory), interacting with each other and themselves [1]. This modelling of neural activity traces its roots back to the seminal works of Wilson and Cowan [20, 21] and Amari [1]. Similar models motivated by these original works have been developed to understand phenomena such as epileptic seizures [22], orientation selectivity in visual cortex [3, 4], spiral waves in disinhibited neocortex [15, 16], and spatio-temporal patterns seen in large scale electroencephalogram (EEG) and magnetoencephalogram (MEG) neuroimaging studies [7, 9].

Techniques for the analysis of continuum population activity with local excitatory and distal inhibitory interactions (so-called Mexican-hat connectivity) have been developed to study spatially periodic and localised states in neural field models, particularly for smooth synaptic kernels [9, 18]. Here we concentrate on neural fields with piece-wise constant kernels, which have been far less studied. The exception to this statement being the work of Herrmann et al. [14]. The scalar two-dimensional neural field model that we consider is given by

$$\frac{\partial u(\boldsymbol{r},t)}{\partial t} = -u(\boldsymbol{r},t) + \int_{\mathscr{D}} w(\boldsymbol{r},\boldsymbol{r}')F(u(\boldsymbol{r}',t))\mathrm{d}\boldsymbol{r}', \tag{1}$$

where $\mathscr{D}$ is a planar domain $\mathscr{D} \subseteq \mathbb{R}^2$. The variable u represents average synaptic activity at position $\boldsymbol{r} \in \mathscr{D}$ at a time $t \in \mathbb{R}^+$. The non-linear function F represents the firing rate of the tissue and is taken to be a Heaviside as in the seminal work of Amari [1], such that $F(u) = H(u-h)$ for some constant threshold h. See [2] for a recent perspective by Amari on the "Heaviside World". Here, the synaptic kernel w describes anatomical connectivity. For mathematical convenience we choose the kernel to depend only on Euclidean distance, so that $w(\boldsymbol{r},\boldsymbol{r}') = w(|\boldsymbol{r}-\mathbf{r}'|)$. It is now of particular interest to consider synaptic connectivity kernels for which explicit analytical progress can be made. In the first instance, let us consider a piece-wise constant rotationally symmetric (Top hat) connectivity defined by

$$w(r) = \begin{cases} w_+ > 0, & r \le \sigma \\ w_- < 0, & r > \sigma \end{cases}, \qquad r = |\boldsymbol{r}|, \tag{2}$$

where w_+ and w_- are constant positive and negative synaptic strength factors respectively. An illustration of a piece-wise constant Top hat function is shown in Fig. 1.

Another natural choice is the piece-wise constant Mexican hat shape given by

$$w(r) = \begin{cases} w_+ > 0, & r \le \sigma_1 \\ w_- < 0, & \sigma_1 < r \le \sigma_2, \\ 0, & r > \sigma_2 \end{cases} \qquad \sigma_1 < \sigma_2\,. \tag{3}$$

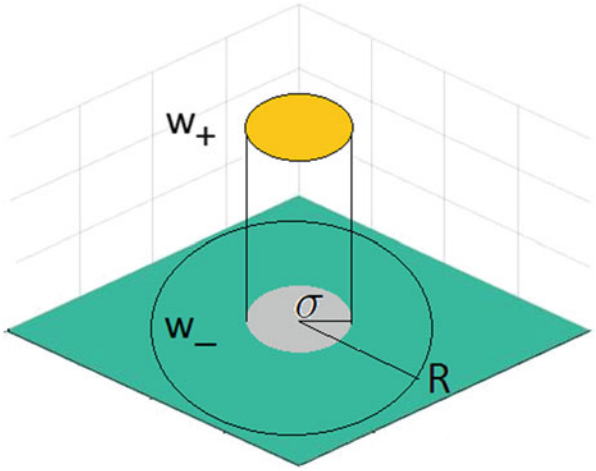

Fig. 1 An illustration of a piece-wise constant Top hat kernel. Synaptic interactions are positive up to a distance σ ($w_+ > 0$) and negative beyond this distance ($w_- < 0$)

In Sect. 2, we show how piece-wise constant caricatures of synaptic connectivity allow for simple calculations relating to localised solutions of neural fields in two-dimensions. Self-consistent equations for stationary solutions of spots are explicitly constructed in Sect. 2.1 and their stability is determined in Sect. 2.2. Here, we find that localised circular spots, obtained using piece-wise constant Mexican kernels, can destabilise to azimuthal instabilities, leading to non-circular patterns with multiple lobes. The numerical solutions beyond a predicted bifurcation point can lead to the generation of labyrinthine structures. Interestingly, a piece-wise constant Top hat kernel is more robust to azimuthal instabilities. Lastly in Sect. 3 we discuss possible extensions of the work in this article.

2 Neural Fields in Circular Geometries: Top Hat Interactions

Here we focus on the construction of rotationally symmetric (spot) solutions for neural fields with piece-wise constant Top hat interactions described by Eq. (2) and determine the stability of these solutions. Following the work of Herrmann et al. [14], we show how explicit solutions, for rotationally symmetric spots, can be easily constructed using simple geometric ideas. We further show that calculation of their stability is straightforward.

2.1 Construction

Stationary solutions $q(\boldsymbol{r})$ of Eq. (1) with Heaviside firing rate satisfy

$$q(\boldsymbol{r}) = \int_{\Omega} \mathrm{d}\boldsymbol{r}' w(\boldsymbol{r} - \boldsymbol{r}'), \tag{4}$$

where $\Omega = \{\boldsymbol{r} \,|\, q(\boldsymbol{r}) > h\}$ represents the area over which the local field is excited. For circularly symmetric spot solutions of radius R we have that $q(\boldsymbol{r}) = U(r)$, where

$$U(r) = \iint_{|\boldsymbol{r}'|<R} \mathrm{d}\boldsymbol{r}' w(|\boldsymbol{r} - \boldsymbol{r}'|), \quad U(R) = h. \tag{5}$$

For the piece-wise constant Top hat kernel given by Eq. (2), we may split the above integral as

$$U(r) = w_+ \iint_{\substack{|\boldsymbol{r}'|<R \\ |\boldsymbol{r}-\boldsymbol{r}'|<\sigma}} \mathrm{d}\boldsymbol{r}' + w_- \iint_{\substack{|\boldsymbol{r}'|<R \\ |\boldsymbol{r}-\boldsymbol{r}'|>\sigma}} \mathrm{d}\boldsymbol{r}'. \tag{6}$$

Introducing the area $A_+(\sigma)$ as follows

$$A_+(\sigma) = \iint_{\substack{|\boldsymbol{r}'|<R \\ |\boldsymbol{r}-\boldsymbol{r}'|<\sigma}} \mathrm{d}\boldsymbol{r}' \Bigg|_{r=R}, \tag{7}$$

means that the self-consistent equation for a spot takes the form

$$h = (w_+ - w_-)A_+(\sigma) + w_- \pi R^2. \tag{8}$$

Here, the area $A_+(\sigma)$ can be calculated in terms of the area of overlap of two circles, one of center $(0, 0)$ and radius R, and the other of center $\boldsymbol{r}$ and radius σ subject to the constraint $|\boldsymbol{r}| = R$. Using the results from the Appendix we find

$$A_+(\sigma) = A(R, \phi_0) + A(\sigma, \phi_1), \tag{9}$$

where $A(r, \phi) = r^2(\phi - \sin\phi)/2$ and

$$\phi_0 = 2\cos^{-1}\left(\frac{2R^2 - \sigma^2}{2R^2}\right), \qquad \phi_1 = 2\cos^{-1}\left(\frac{\sigma}{2R}\right), \qquad R > \frac{\sigma}{2}. \tag{10}$$

For example, for the special case that $R = \sigma$ and $h = 0$, it is easy to show

$$A_+(\sigma) = 2A(R, 2\pi/3) = R^2(2\pi/3 - \sqrt{3}/2). \tag{11}$$

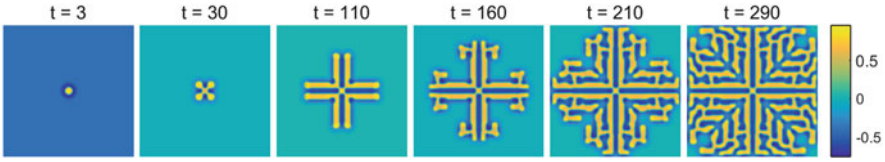

Fig. 2 Direct numerical simulations of a spreading pattern governed by the space-time model (1) with a radially symmetric piece-wise constant Mexican hat kernel on a domain of size $[-L, L] \times [-L, L]$. Parameter values: $w_+ = 0.1$, $w_- = -0.004$, $h = 0.1$, $\sigma_1 = 2$, $\sigma_2 = 10$, $L = 100$. Here, yellow and blue regions represent the excited (high activity) and quiescent states (low activity), respectively

Using Eq. (8), we obtain the ratio

$$\frac{w_+}{w_-} = 1 - \frac{\pi}{(2\pi/3 - \sqrt{3}/2)}, \tag{12}$$

which recovers the results in [14].

Another natural piece-wise constant choice for synaptic connectivity is the piece-wise constant Mexican hat shape given by (3). Using a similar argument to the one used for the piece-wise constant Top hat connectivity, we find the self consistent equation for a localised spot

$$h = (w_+ - w_-)A_+(\sigma_1) + w_- A_+(\sigma_2). \tag{13}$$

In Fig. 2, we show the results of direct numerical simulations at fixed times for a neural field with a piece-wise constant Mexican hat kernel. These simulations show the emergence of an exotic mazelike pattern with a four fold symmetry.

A plot of the theoretical spot radius as a function of the firing threshold is shown in Fig. 3. Here we see two branches of solutions, so that a wide and narrow spot can co-exist. Direct numerical simulations show, for the chosen parameters, that the wider one is stable. Moreover, the wide spot appears to be stable to deformations that change the radius according to $R \to R + \epsilon \cos m\theta$, where $\theta \in [0, 2\pi)$, $m \in \mathbb{N}$ and $|\epsilon| \ll 1$. In this setting, the simulations in Fig. 2 suggest that the spot is unstable to an azimuthal instability with $m = 4$. We shall investigate this robustness to *azimuthal instabilities* in more detail in the next sub-section. Note that, similar exotic patterns with a smooth Mexican hat connectivity have been found and discussed in [6, 8, 18].

The numerical evolution of (1) was performed using two-dimensional fast Fourier transforms to compute convolutions, discretising space into 2^9 points on a periodic domain, and evolving the resultant set of ordinary differential equations using MATLAB 2015a with a standard non-stiff *ode45* solver. For a further discussion see [8, 19].

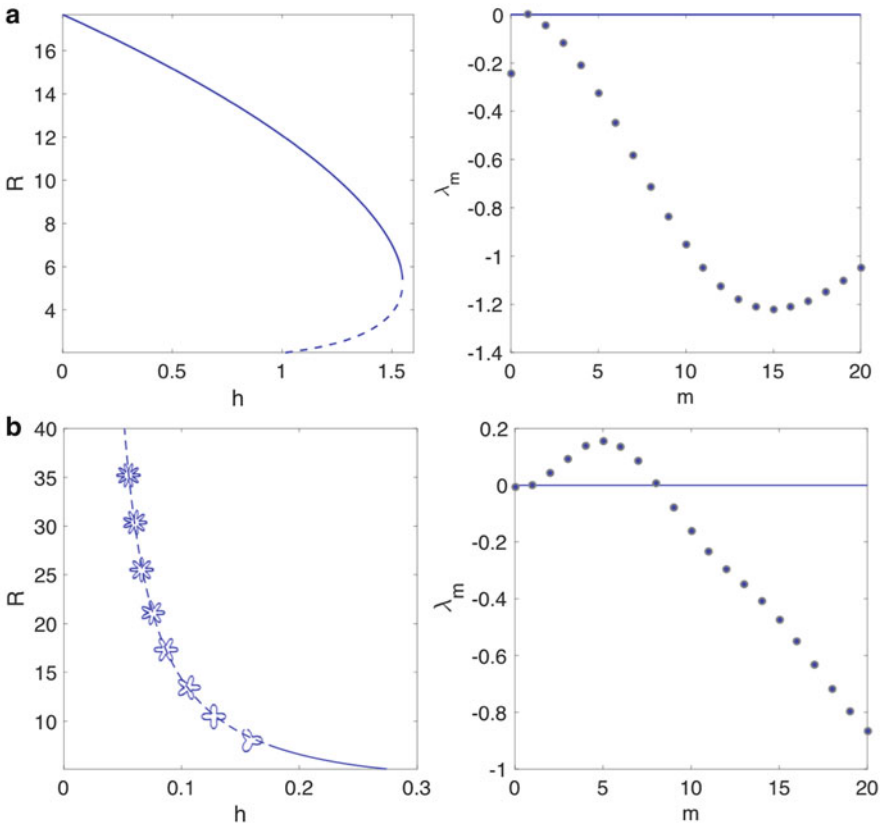

Fig. 3 Bifurcation diagrams for radius R as a function of the threshold h. (**a**) Piece-wise constant Top hat kernel, with the right panel showing the spectrum for $h = 0.1$. Parameters are $w_+ = 0.08$, $w_- = -0.002$, $\sigma = 4$ with constraint $2R > \sigma$. (**b**) Piece-wise constant Mexican hat kernel, with the right panel showing the spectrum for $h = 0.1$. Parameters are $w_+ = 0.1$, $w_- = -0.004$, $\sigma_1 = 2$, $\sigma_2 = 10$ with constraint $2R > \sigma_2 > \sigma_1$

2.2 *Stability*

To determine the linear stability of a spot we follow [5, 6, 8, 18] and write $u(r, t) = U(r) + \mathrm{e}^{\lambda t}\cos(m\phi)\delta u(r)$ where $0 < \delta u \ll 1$ and $m \in \mathbb{N}$. Expanding (1) to first order gives

$$(\lambda + 1)\delta u(r) = \int_0^{2\pi} \mathrm{d}\phi \cos(m\phi) \int_0^{\infty} r' \mathrm{d}r' w(|\boldsymbol{r} - \boldsymbol{r}'|) H'(U(r') - h)\delta u(r'), \quad (14)$$

where we write $|\boldsymbol{r}-\boldsymbol{r}'| = \sqrt{r^2+r'^2-2rr'\cos(\phi-\phi')}$ with $\boldsymbol{r} = (r,\phi)$ and $\boldsymbol{r}' = (r',\phi')$. Since H' occurs under an integral, we can formally write

$$H'(U(r)-h) = \frac{\delta(r-R)}{|U'(R)|}, \tag{15}$$

to yield

$$(\lambda+1)\delta u(r) - \delta u(R)\frac{R}{|U'(R)|}\int_0^{2\pi} \mathrm{d}\phi\cos(m\phi)\; w(|\boldsymbol{r}-\boldsymbol{r}'|)\big|_{r'=R} = 0. \tag{16}$$

By setting $r = R$ and demanding non-trivial solutions we obtain an equation for the eigenvalues λ in the form $\mathscr{E}_m(\lambda) = 0$, $m \in \mathbb{N}$, where

$$\mathscr{E}_m(\lambda) = \lambda + 1 - \frac{R}{|U'(R)|}\int_0^{2\pi} \mathrm{d}\phi\cos(m\phi)\; w(|\boldsymbol{r}-\boldsymbol{r}'|)\big|_{r'=r=R}. \tag{17}$$

A localised spot solution will be stable if $\lambda_m < 0$ for all $m \in \mathbb{N}$, where λ_m is a zero of $\mathscr{E}_m(\lambda)$. Note that $\mathscr{E}_1(0) = 0$ is always true since a radially symmetric solution $q(r,\phi) = U(r)$ is invariant under the transformation $\phi \to \phi + \phi_0$, $\phi_0 \in [0,2\pi)$. Once more we emphasise that the nature of constant piece-wise kernels substantially simplifies the mathematical expressions presented above. For example for the piece-wise Top hat function given by (2) it is simple to show that

$$U'(R) = \frac{\sigma(w_- - w_+)}{R}\sqrt{4R^2-\sigma^2}, \tag{18}$$

and

$$\int_0^{2\pi} \mathrm{d}\phi\cos(m\phi)\; w(|\boldsymbol{r}-\boldsymbol{r}'|)\big|_{r'=r=R} = 2\left(\frac{w_+ - w_-}{m}\right)\sin m\phi^*, \tag{19}$$

where ϕ^* is the smaller of the two roots of the equation $R\sqrt{2(1-\cos\phi)} = \sigma$ for $\phi \in [0,2\pi)$. In Fig. 3, plots of the radius R as a function of the threshold parameter h, and the spectra of selected profiles are shown for the piece-wise constant Top hat (Fig. 3a) and Mexican hat (Fig. 3b) kernels. Our linear stability analysis of the stationary circular solutions for the piece-wise constant Top hat kernel shows that lower (dashed) branch of solutions is unstable to uniform changes (expansion or contraction) of size ($m = 0$) and the upper (solid) branch is stable. Here, from Eqs. (17)–(19), it is straightforward to show that piece-wise constant Top hat kernels do not support azimuthal instabilities of spots with modes $m \geq 2$. However, the piece-wise constant Mexican hat kernel readily supports azimuthal instabilities of various modes ($m \geq 2$). These results are consistent with those previously found by several authors for smooth Mexican hat kernels, as in [5, 10, 11, 18].

For further details on pattern formation in planar neural fields with smooth kernels and a Heaviside firing rate see [5, 8, 18].

3 Discussion

In this article we have shown that the analysis of the Amari model simplifies even further for the choice of piece-wise constant synaptic kernels. These kernels allow the analysis of localised states in the form of spots and their azimuthal instabilities that can lead to spreading labyrinthine structures.

There are several possible extensions of the work presented in this article. Perhaps the most obvious extension is to expand the analysis to tackle bounded domains with imposed boundary conditions. Since the pioneering work of Amari [1], neural field models have usually been considered to describe the behaviour of tissue in infinite domains, and solutions on bounded domains have drawn very little attention. Focusing on the Dirichlet boundary conditions, the key mathematical idea to treat this has recently been formulated and discussed in [13].

Another extension would be to consider doubly periodic solutions with $u(\boldsymbol{r} + \boldsymbol{l}_{1,2}, t) = u(\boldsymbol{r}, t)$, for linearly independent vectors $\boldsymbol{l}_{1,2} \in \mathbb{R}^2$. From Eq. (4) the doubly periodic stationary solution is given by

$$U(r) = \sum_{m,n\in\mathbb{Z}} \iint_{|\boldsymbol{r}'+m\boldsymbol{l}_1+n\boldsymbol{l}_2|<R} w\left(|\boldsymbol{r}-\boldsymbol{r}'|\right) \mathrm{d}\boldsymbol{r}', \tag{20}$$

subject to the constraint $U(R) = h$. In Fig. 4, numerical solutions of the full neural field model show the evolution of patterns starting from doubly periodic solutions. For example in Fig. 4a, we observe destabilisation of a hexagonal tiling into an overlapping concentric circular-like pattern. In Fig. 4b the pattern destabilises to large spots that are compressed and trapped by surrounding small spots. We see a regularly deforming pattern which looks like a chequered flag in Fig. 4c, and lastly the initial conditions destabilise to a star-like pattern in Fig. 4d.

A further analysis of doubly periodic solutions will be presented elsewhere, including the use of numerical continuation methods to determine solutions and their stabilities by considering the ideas in [19].

Appendix: Circular Geometry for a Top Hat Kernel

Consider a portion of a disk whose upper boundary is an (circular) arc and whose lower boundary is a chord making a central angle $\phi_0 < \pi$, illustrated as the shaded region in Fig. 5a. The area $A = A(r_0, \phi_0)$ of the (shaded) segment is then simply given by the area of the circular sector (the entire wedge-shaped portion) minus the

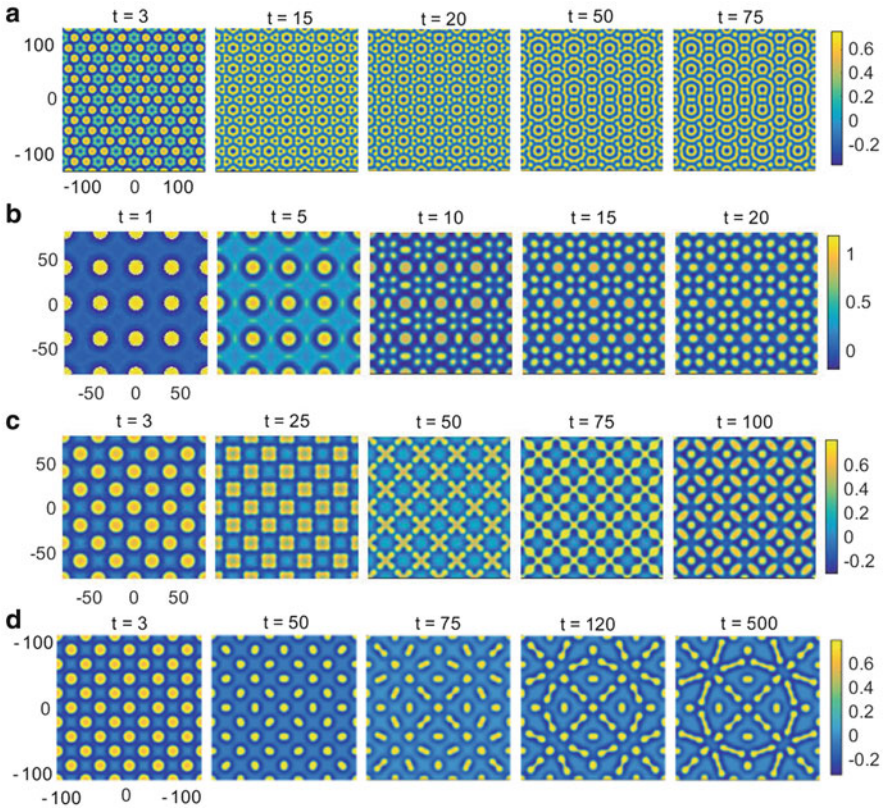

Fig. 4 Various space time simulations for a piece-wise constant Mexican hat kernel. Panels (**a**) and (**b**) are simulated with a sigmoidal firing rate function of the form $F(u) = 1/(1+\mathrm{e}^{-\mu(u-h)})$. Panels (**c**) and (**d**) are simulated with a Heaviside firing rate. Parameters are (**a**) $w_+ = 0.1, w_- = -0.004$, $\mu = 6, \sigma_1 = 2, \sigma_2 = 10, h = 0.12, L = 150$, (**b**) $w_+ = 0.1, w_- = -0.004, \mu = 10, \sigma_1 = 2$, $\sigma_2 = 10, h = 0.23, L = 80$, (**c**) $w_+ = 0.1, w_- = -0.004, \sigma_1 = 2, \sigma_2 = 10, h = 0.14, L = 80$, (**d**) $w_+ = 0.1, w_- = -0.004, \sigma_1 = 2, \sigma_2 = 10, h = 0.283, L = 100$

area of an isosceles triangle, namely

$$A(r_0, \phi_0) = \frac{1}{2} r_0^2 \left(\phi_0 - \sin \phi_0\right). \tag{21}$$

The area of the overlap of two circles, as illustrated in Fig. 5b, can be constructed as the total area of $A(r_0, \phi_0) + A(r_1, \phi_1)$. To determine the angles $\phi_{0,1}$ in terms of the centers, (x_0, y_0) and (x_1, y_1), and radii, r_0 and r_1, of the two circles we use the cosine formula that relates the lengths of the three sides of a triangle formed by joining the centers of the circles to a point of intersection. We denote distance between the two

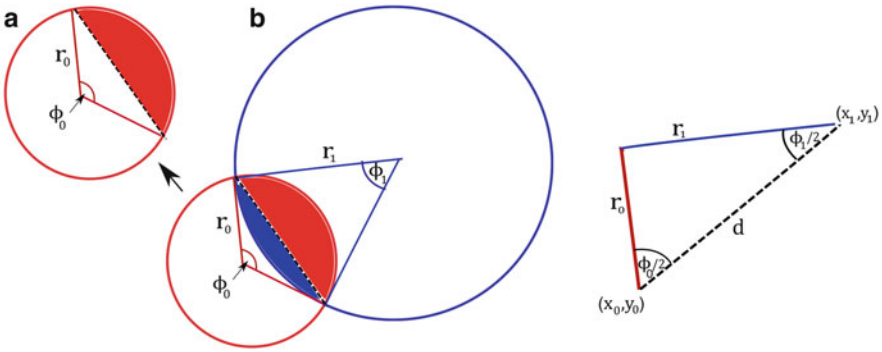

Fig. 5 The area of the total shaded segment is $r_0^2(\phi_0 - \sin\phi_0)/2$ (**a**). Overlap of two circles shows the area of active region (**b**)

centers by d where $d^2 = (x_0 - x_1)^2 + (y_0 - y_1)^2$ so that

$$r_1^2 = r_0^2 + d^2 - 2r_0 d\cos(\phi_0/2), \qquad r_0^2 = r_1^2 + d^2 - 2r_1 d\cos(\phi_1/2). \tag{22}$$

Hence the angles are given by

$$\phi_0 = 2\cos^{-1}\left(\frac{r_0^2 + d^2 - r_1^2}{2r_0 d}\right), \qquad \phi_1 = 2\cos^{-1}\left(\frac{r_1^2 + d^2 - r_0^2}{2r_1 d}\right). \tag{23}$$

References

1. Amari, S.: Dynamics of pattern formation in lateral-inhibition type neural fields. Biol. Cybern. **27**(2), 77–87 (1977)
2. Amari, S.: Heaviside world: excitation and self-organization of neural fields. In: Neural Fields: Theory and Applications. Springer, Berlin, Heidelberg (2014)
3. Bressloff, P.C., Carroll, S.R.: Spatiotemporal dynamics of neural fields on product spaces. SIAM J. Appl. Dyn. Syst. **13**(4), 1620–1653 (2014)
4. Bressloff, P.C., Carroll, S.R.: Laminar neural field model of laterally propagating waves of orientation selectivity. PLoS Comput. Biol. **11**(10), e1004545 (2015)
5. Bressloff, P.C., Coombes, S.: Neural 'Bubble' dynamics revisited Cogn. Comput. **5**(3), 281–294 (2013)
6. Coombes, S.: Waves, bumps, and patterns in neural field theories. Biol. Cybern. **93**(2), 91–108 (2005)
7. Coombes, S.: Large-scale neural dynamics: simple and complex. NeuroImage **52**(3), 731–739 (2010)
8. Coombes, S., Schmidt, H., Bojak, I.: Interface dynamics in planar neural field models. J. Math. Neurosci. **2**(1), 1 (2012)
9. Coombes, S., Beim Graben, P., Potthast, R., Wright, J.: Neural Fields. Springer, Berlin (2014)
10. Coombes, S., Schmidt, H., Avitabile, D.: Spots: breathing, drifting and scattering in a neural field model. In: Neural Fields, pp. 187–211. Springer, Berlin (2014)

11. Ermentrout, G.B., Folias, S.E., Kilpatrick, Z.P.: Spatiotemporal pattern formation in neural fields with linear adaptation. In: Neural Fields, pp. 119–151. Springer, Berlin (2014)
12. Fischl, B., Dale, A.M.: Measuring the thickness of the human cerebral cortex from magnetic resonance images. Proc. Natl. Acad. Sci. **97**(20), 11050–11055 (2000)
13. Gökçe, A., Avitabile, D., Coombes, S.: The dynamics of neural fields on bounded domains: an interface approach for Dirichlet boundary conditions. J. Math. Neurosci. **7**(1), 12 (2017)
14. Herrmann, J. M., Schrobsdorff, H., Geisel, T.: Localized activations in a simple neural field model. Neurocomputing **65**, 679–684 (2005)
15. Huang, X., Troy, W.C., Yang, Q., Ma, H., Laing, C.R., Schiff, S.J., Wu, J.-Y.: Spiral waves in disinhibited mammalian neocortex. J. Neurosci. **24**(44), 9897–9902 (2004)
16. Laing, C.R.: Spiral waves in nonlocal equations. SIAM J. Appl. Dyn. Syst. **4**(3), 588–606 (2005)
17. Nunez, P.L., Srinivasan, R.: Electric Fields of the Brain: The Neurophysics of EEG. Oxford University Press, Oxford (2006)
18. Owen, M.R., Laing, C.R., Coombes, S.: Bumps and rings in a two-dimensional neural field: splitting and rotational instabilities. New J. Phys. **9**(10), 378 (2007)
19. Rankin, J., Avitabile, D., Baladron, J., Faye, G., Lloyd, D.J.:. Continuation of localized coherent structures in nonlocal neural field equations. SIAM J. Sci. Comput. **36**(1), B70–B93 (2014)
20. Wilson, H.R., Cowan, J.D.: Excitatory and inhibitory interactions in localized populations of model neurons. Biophys. J. **12**(1), 1 (1972)
21. Wilson, H.R., Cowan, J.D.: A mathematical theory of the functional dynamics of cortical and thalamic nervous tissue. Kybernetik **13**(2), 55–80 (1973)
22. Zhao, X., Robinson, P.: Generalized seizures in a neural field model with bursting dynamics. J. Comput. Neurosci. **39**(2), 197–216 (2015)